Surface plasmon polaritons in curved chains of metal nanoparticles

Ilia L. Rasskazov[*]

L. V. Kirensky Institute of Physics and Siberian Federal University, Krasnoyarsk, Russia

Sergei V. Karpov

L. V. Kirensky Institute of Physics, Siberian State Aerospace University and Siberian Federal University, Krasnoyarsk, Russia

Vadim A. Markel[†]

Departments of Radiology and Bioengineering and the Graduate Group in Applied Mathematics and Computational Science, University of Pennsylvania, Philadelphia, Pennsylvania 19104, USA

We investigate numerically the propagation of steady-state monochromatic surface plasmon polaritons (SPPs) in curved chains of metal nanoparticles of various spheroidal shapes. We discuss the SPP propagation (decay of the amplitude), the polarization conversion due to coupling of orthogonally polarized SPPs, and the electromagnetic field localization in the near-field vicinity of a chain.

I. INTRODUCTION

Surface plasmon polaritons (SPPs) that can be excited under a variety of different physical scenarios in chains of metal nanoparticles (plasmonic chains) is a topic of vigorous ongoing research [1–8]. Applications related to wave guiding, nanoscale manipulation and transport of optical information, and minituarization of optoelecronic elements have been envisioned. The laws governing the propagation and decay of steady-state, monochromatic SPPs in infinite or semi-infinite linear, perfectly periodic chains are well understood at present [9–13]. Although a perfectly periodic chain is obviously an idealization, it was shown that weak disorder [9,14] or double periodicity [15] do not have a dramatic effect on long-range SPP propagation. Dispersion relations and transient processes (wave-packet transmission) in plasmonic chains have also been studied [16–19]. In particular, it was found that chains of spherical particles can not support the propagation of well-formed wave packets due to the flatness of the corresponding dispersion curves. However, this problem can be alleviated by using chains of nonspherical particles such as prolate or oblate spheroids [13,17], for instance. Chains of this type can serve as broadband SPP waveguides. The latter fact motivates our interest in various types of chains composed of nonspherical plasmonic particles.

In the majority of previous publications on the subject, straight linear chains have been considered. However, curved chains are of both theoretical interest and of practical importance. It was shown experimentally and in simulations [20,21] that parabolic chains of nanoparticles can focus and direct SPPs. In these references, the parabolic chains were used as reflectors and collimators of SPPs that propagate on the metal/vacuum interface rather than as the structures that *support* the SPPs. However, in a separate investigation [22],

the propagation of SPPs directly in curved plasmonic chains placed above a gold substrate was demonstrated in simulations. The finding that SPPs can propagate in curved chains is important because it is not clear *a priori* that a significant curvature of a chain would not result in strong radiative losses or in suppression of the field localization effect.

In this paper, we consider the propagation of SPPs in curved chains of various shape with a special emphasis on polarization effects. In this respect, there exists a qualitative difference between straight and curved chains. In straight chains, different orthogonal polarizations of the SPPs are decoupled. In curved chains, this is no longer so. Coupling of differently polarized SPPs results in new physical effects that are not observed in linear chains, such as polarization conversion. Below, we present a numerical investigation of steady-state, monochromatic SPPs in curved chains of various types (sharp and smooth corners and quarter-circles). We consider chains made of spheroids of varying shape and aspect ratio and study the amplitude decay, the polarization conversion, and the field localization effects.

In the simulations reported below, we have used a number of approximations and simplifying assumptions. First, we use the point-dipole approximation, which is the simplest theoretical model that can still capture some important physical effects that occur in plasmonic chains. However, the dipole approximation is expected to fail when the interparticle spacing is too small. An alternative to the dipole approximation is either the use of generalized Mie solution (the coupled-multipole methods [23–25]) or numerical methods of general applicability, such as finite difference or finite element methods [7,18,26]. We note that the couple-multipole methods are especially well-suited when the particles are made of new low-loss materials [7,27] in which several multipole moments (Mie resonances) are excited and the dipole approximation is clearly insufficient, regardless of the interparticle distance. However, extension of the generalized Mie solution beyond the case of spherical particles is problematic and has not been attempted to the best of our knowledge. On the other hand, we are specifically interested in nonspherical particles. The general-applicability numerical methods are also limited

————

[*]While working on this paper, I. L. Rasskazov was a visiting scientist at the Department of Bioengineering, University of Pennsylvania, USA; il.rasskazov@gmail.com

[†]vmarkel@mail.med.upenn.edu

in utility due to their high computational complexity. Due to these reasons, we chose to stay within the framework of the dipole approximation while keeping the interparticle distance reasonably large. It should be noted that the validity of this approach was confirmed in simulations [18] and in a combination of simulations and experiments [20–22].

Second, a remark is needed regarding the shape of the nanoparticles that we use in the simulations. Although we discuss spheroids, it is neither practically possible nor important for us that these particles are of perfect spheroidal shape. What comes up in the simulation as an important parameter is the *depolarization factor*. This quantity can be, to some level of approximation, be introduced not only for perfect spheroids but also for other shapes, such as truncated cylinders for example.

Third, we consider the plasmonic chains in free space and, therefore, do not account for the presence of substrate or a host medium. Coupling of the SPPs in a chain and a substrate results in a number of new phenomena [4,15,28,29]. In particular, the SPPs propagating in the chain and on the interface become coupled and can exchange energy. A chain SPP that is perfectly contained to the chain can become leaky near an interface and radiate into selected angles. Polarization effects become also more complex. An interesting finding is that reflective metal interfaces do not necessarily suppress chain SPPs but can even enhance transmission, in spite of the additional Ohmic losses associated with substrate [4]. In this study, we restrict our attention to chains in free space, which allows us to focus on a few physical effects such as polarization conversion. Experimentally, the model we use is relevant to substrates whose refractive index is not too much different from unity at the working frequency, such as the ordinary glass. As for the host medium, its primary effect is to shift the spectral positions of the optical resonances of individual particles.

The reminder of this paper is organized as follows. In Sec. II, we explain the physical model used in numerical simulations. Numerical results for transmission and polarization effects are given in Sec. III and results for field localization in Sec. IV. Section V summarizes the results obtained.

II. THEORETICAL MODEL

We consider propagation of SPPs in curved chains of spheres and prolate or oblate spheroids (ellipsoids of revolution) of nanoscale dimensions. The dipole approximation is used to model the SPP propagation. We work in the frequency domain and use the phasor convention $\exp(-i\omega t)$; the latter exponential factor is suppressed in all formulas. The vacuum wave number at the working frequency is denoted by $k = \omega/c$. In the reminder of this section, we describe the geometry of the chains used (Sec. II A), outline the basic formulas of the dipole approximation (Sec. II B) and adduce the required formulas for the polarizability tensors of the nanospheroids with the account of appropriate dynamic corrections [30] (Sec. II C).

A. Geometry

The spheroids comprising a given chain are assumed to be identical, with the longer and shorter semiaxes denoted by a and b. The aspect ratio and the eccentricity of a spheroid are

defined by

$$\xi = b/a \leqslant 1, \quad e = \sqrt{1 - \xi^2}, \tag{1}$$

where $b \leqslant a$ and the equality holds in the particular case of spheres. Detailed information on all the chain geometries that we have used in the simulations is provided in Fig. 1. Specifically, we have considered chains built from N particles, which can be spheres, oblate or prolate spheroids. The centers of all spheroids lie in the plane $z = 0$ and one of the principal axes of each spheroid is parallel to the Z axis. In addition, the particles are oriented in space so that their axes of symmetry are contained in the XY plane. In the case of prolate spheroids, the axes of symmetry (shown by dashed lines in Fig. 1) are perpendicular to the chain, while in the case of oblate spheroids they are parallel.

According to their overall shape, the chains can be classified as either corners, smooth corners or quarter-circles. All these cases are shown in Fig. 1. In the case of smooth corners, the particles are assembled into chains so that their centers are connected by a curve in the XY plane, which consists of two straight segments oriented parallel to the X and Y axes and connected by a circular arc with the central angle $\pi/2$. In the case of a corner, the circular arc is absent and the two straight segments connect at a vertex. In the case of a quarter-circle, the straight segments are absent and only a circular arc is used. The distance h between the neighboring particle centers measured *along the curve* is fixed. If we denote the number of particles connected by the circular arc by N_c, then the arc's radius of curvature is $R = 2h(N_c - 1)/\pi$. We note that in all cases where a circular arc was used, we have $h \ll R$. Correspondingly, the *center-to-center* distance between the neighboring particles is very close to h.

The specific geometrical parameters used in the simulations are as follows. The total number of particles in all chains is $N = 1001$. In the case of corners, there is one corner particle at the vertex and $(N - 1)/2 = 500$ particles in each straight segment connected to the vertex. In the case of smooth corners, there are $N_c = (N + 1)/2 = 501$ particles on the circular arc segment and $(N - 1)/4 = 250$ particles in each straight segment. In the case of quarter-circles, we have $N_c = N$.

Further, we have fixed the shorter semiaxis of all spheroids to $b = 8$ nm and the inter-particle spacing *along the curve* to $h = 24$ nm. The longer axes of the spheroids vary. With these parameters, the total length of the chain is $L = 24$ μm and the radius of curvature of the circular arcs used is $R \approx 7.64$ μm in the case of smooth corners and 15.28 μm for the quarter-circles (twice as large).

B. Dipole approximation

Consider a chain of N spheroids centered at the points $\mathbf{r}_n$ and characterized by the tensor polarizability α_n, where $n = 1, \ldots, N$. Even though all spheroids in a given chain are assumed to be identical, the tensors α_n can be different because the spheroids are, in general, differently oriented in the XY plane. In our model, each spheroid can be obtained from another spheroid in the same chain by a rotation about the Z axis and translation in the XY plane. (Note that this is different from the model of Ref. [22], where the nanospheroids in a given chain differed only by translation, while their axes
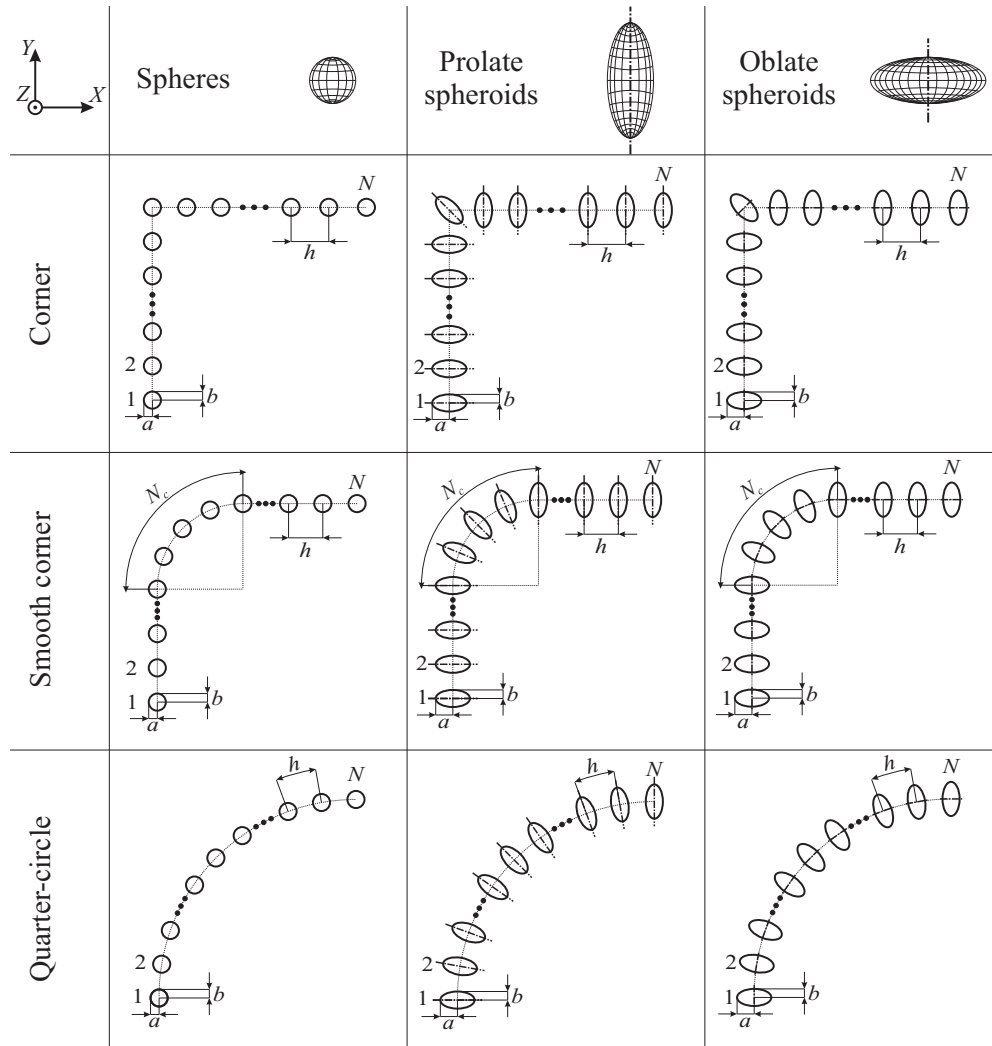
FIG. 1. Schematic top view of all chains used in the simulations. Note that prolate and oblate spheroids can not be distinguished when viewed from top. However, the axes of symmetry in each case are oriented differently with respect to the chain, as is shown by the dashed lines. The total number of particles in a chain is N and the number of particles connected by the circular arc segment of the chain is N_c ($N_c = 0$ for corners). The longer and shorter semiaxes of the spheroid are denoted by a and b. The interparticle distance *measured along the curve* is h.

were kept parallel to the axes of the laboratory frame.) In the dipole approximation, the dipole moments $\mathbf{d}_n$ of the spheroids are coupled to each other and to the external electric field by the coupled-dipole equation [31]:

$$\mathbf{d}_n = \alpha_n \left(\mathbf{E}_n + \sum_{m \neq n} G_{nm} \mathbf{d}_m \right). \tag{2}$$

Here, $\mathbf{E}_n$ is external (incident) electric field at the center of nth nanoparticle and G_{nm} is the free-space frequency-domain Green's tensor for the electric field whose components are given explicitly elsewhere [31].

To quantify the SPP propagation along the chain, we use the formalism of normalized Green's functions [9]. From the linearity of (2), it is clear that the solution can be written as

$$\mathbf{d}_n = \sum_m \mathcal{D}_{nm} \mathbf{E}_m, \tag{3}$$

where $\mathcal{D}_{nm}$ is the Green's tensor of the chain, which can be obtained numerically (or, in the case of infinite [9] or semi-infinite [10] linear chains, analytically). Here we consider

finite curved chains for which an analytical solution is not available. Correspondingly, we will compute $\mathcal{D}_{nm}$ numerically by standard methods of linear algebra.

Now assume that the chain is illuminated by a localized (near-field) external source, which creates a fixed and given amplitude $\mathbf{E}_1$ of the electric field at the center of the first particle in the chain and negligibly small incident field elsewhere. In this case, (3) takes the form $\mathbf{d}_n = \mathcal{D}_{n1} \mathbf{E}_1$. We then define the *normalized scalar* Green's function as

$$\mathcal{F}_n = \frac{|\mathcal{D}_{n1} \mathbf{E}_1|}{|\mathcal{D}_{11} \mathbf{E}_1|}, \tag{4}$$

where $|\mathbf{x}| = \sqrt{\mathbf{x}^* \cdot \mathbf{x}}$ for any three-dimensional complex vector $\mathbf{x}$. Since $\mathcal{F}_n$ is a positive scalar, we can view it as the measure of SPP decay. In particular, we will refer to $\mathcal{F}_N$ as to the transmission of the chain as a whole. It should be kept in mind that the function $\mathcal{F}_n$, as defined, is not independent of $\mathbf{E}_1$. Indeed, the transmission of a given chain can depend on the incident polarization.

Note also that the scalar Green's function $\mathcal{F}_n$ is not directly measurable because any realistic external illumination can not be strictly localized on the first particle of a chain. However, we have verified that $\mathcal{F}_n$ is very close to the directly measurable quantity $|\mathbf{d}_n|/|\mathbf{d}_1|$, where $\mathbf{d}_n$ is obtained by solving (2) with a more realistic external illumination pattern, as long as near-field excitation is used. We have checked this statement by taking $\mathbf{E}_n$ to be the field of a radiating dipole placed in close proximity (that is, at a distance $\sim h$) of the first particle in a chain and performing the relevant computations numerically.

C. Polarizability of a spheroid

The polarizability tensor of the n-th spheroid in a chain can be written as

$$\alpha_n = \alpha_\perp \mathbb{I} + (\alpha_\parallel - \alpha_\perp)\hat{\mathbf{u}}_n \otimes \hat{\mathbf{u}}_n, \qquad (5)$$

where $\mathbb{I}$ is the identity tensor, $\alpha_\perp$ and $\alpha_\parallel$ are the principal values of α_n and $\hat{\mathbf{u}}_n$ is the unit vector parallel to the spheroid axis of symmetry. In the case when the host medium is vacuum, $\alpha_\parallel$ and $\alpha_\perp$ are given by the formulas

$$\frac{1}{\alpha_{\parallel,\perp}} = \frac{3\xi^p}{b^3}\left(\nu_{\parallel,\perp} + \frac{1}{\epsilon - 1}\right) - \frac{k^2}{b}\beta_{\parallel,\perp} - \frac{2ik^3}{3}, \quad (6)$$

where $p = 1$ for prolate spheroids, $p = 2$ for oblate spheroids, $\nu_{\parallel,\perp}$ are the static depolarization factors, $k^2\beta_{\parallel,\perp}/b$ are the second-order (in k) dynamic corrections to the inverse polarizability [30], and the term $-2ik^3/3$ is the third-order dynamic correction (the first nonvanishing radiative correction [32]). We note that first-order corrections, that is, terms of the order of $O(k)$ are absent in (6).

The static depolarization factors are given by the following formulas. For prolate spheroids,

$$\nu_\parallel = g^2(e)\left(\frac{1}{2e}\ln\frac{1+e}{1-e} - 1\right), \quad \nu_\perp = \frac{1 - \nu_\parallel}{2}, \quad (7)$$

and for oblate spheroids,

$$\nu_\perp = \frac{g(e)}{2e^2}\left[\frac{\pi}{2} - \arctan g(e)\right] - \frac{g^2(e)}{2}, \quad \nu_\parallel = 1 - 2\nu_\perp. \qquad (8)$$

Here,

$$g(e) = \sqrt{1/e^2 - 1} = \xi/\sqrt{1 - \xi^2}. \qquad (9)$$

Note that for both prolate and oblate spheroids, $\nu_\parallel + 2\nu_\perp = 1$. The second-order dynamic corrections are of the form [30]

$$\beta_\parallel = \frac{3}{4}\begin{cases} \xi\left(\frac{1+e^2}{1-e^2}\nu_\parallel + 1\right) & \text{(prolate)} \\ (1 - 2e^2)\nu_\parallel + 1 & \text{(oblate)} \end{cases} \qquad (10)$$

and

$$\beta_\perp = -\frac{\beta_\parallel}{2} + \frac{3\xi}{2e}\begin{cases} \frac{1}{2}\ln\frac{1+e}{1-e} & \text{(prolate)} \\ \arcsin(e) & \text{(oblate)} \end{cases}. \qquad (11)$$

In the last formula, an appropriate expression for $\beta_\parallel$ from (10) must be used, depending on whether the spheroid is prolate or oblate.

Finally, we need to define the complex permittivity of spheroids, ϵ. To this end, we use the Drude formula

$$\epsilon = \epsilon_0 - \frac{\omega_p^2}{\omega(\omega + i\gamma)}, \qquad (12)$$

where ω_p is the plasma frequency, γ is the Drude relaxation constant, and $\epsilon_0 - 1$ is the contribution due to the interband transitions. In simulations, we have used the experimental parameters for silver, viz. $\omega_p/\gamma = 526.3$ and $\epsilon_0 = 5.0$. We did not modify the bulk permittivity of silver to account for the finite size effects.

III. TRANSMISSION AND POLARIZATION EFFECTS

In this section, we study transmission and polarization properties of the chains shown in Fig. 1. We will consider propagation of SPPs at several excitation frequencies and for different shapes of spheroids. We will also consider two different linear polarizations of the incident electric field: along the X and Y axes. In the first case (polarization along X), the SPP is, initially, polarized transversely to the chain. Upon propagation, the linear transverse polarization can be partially converted to longitudinal polarization. As a result, the SPP polarization at the intermediate particles in the chain is, generally, elliptical. Similar situation takes place in the case of the incident polarization along Y, when a longitudinally-polarized SPP is partially converted to a transversely polarized SPP. We note that the above polarization effects are absent in linear chains wherein the transverse and longitudinal SPPs are completely decoupled. In the case of curved chains, the polarization phenomena are particularly complicated because the transverse and longitudinal SPPs have different decay rates and different laws of dispersion.

To quantify the polarization conversion effects, we adopt the following notations. In the case of incident polarization along the X axis, we write $\mathbf{d}_n = \hat{\mathbf{x}}d_n^\parallel + \hat{\mathbf{y}}d_n^\perp$. Analogously, for incident polarization along the Y axis, we write $\mathbf{d}_n = \hat{\mathbf{x}}d_n^\perp + \hat{\mathbf{y}}d_n^\parallel$. Here, $d_n^\perp$ and $d_n^\parallel$ are projections of the vector $\mathbf{d}_n$ onto the directions that perpendicular and parallel to the incident polarization, respectively. We then define the depolarization ratio at nth spheroid as

$$\delta_n = d_n^\perp/d_n^\parallel. \qquad (13)$$

In particular, $\delta_n = 0$ or $\delta_n = \infty$ corresponds to linear polarizations, while $\delta_n = 1$ corresponds to circular polarization.

We start with the results for corner-shaped chains, which are shown in Fig. 2. Propagation in the first straight segment of the chain is similar to propagation in a linear chain, as long as the point of observation is sufficiently far from the vertex. The normalized scalar Green's function $\mathcal{F}_n$ decays either exponentially, if the excitation frequency is close to the resonance frequency of an individual spheroid, or drops sharply and then undergoes slow algebraic decay if the excitation is off-resonance. The resonance frequency for noninteracting spheroid can be found by solving the equation

$$3\xi^p\left[\nu_{\parallel,\perp} + \text{Re}\frac{1}{\epsilon(\omega) - 1}\right] = \left(\frac{\omega b}{c}\right)^2\beta_{\parallel,\perp} \qquad (14)$$
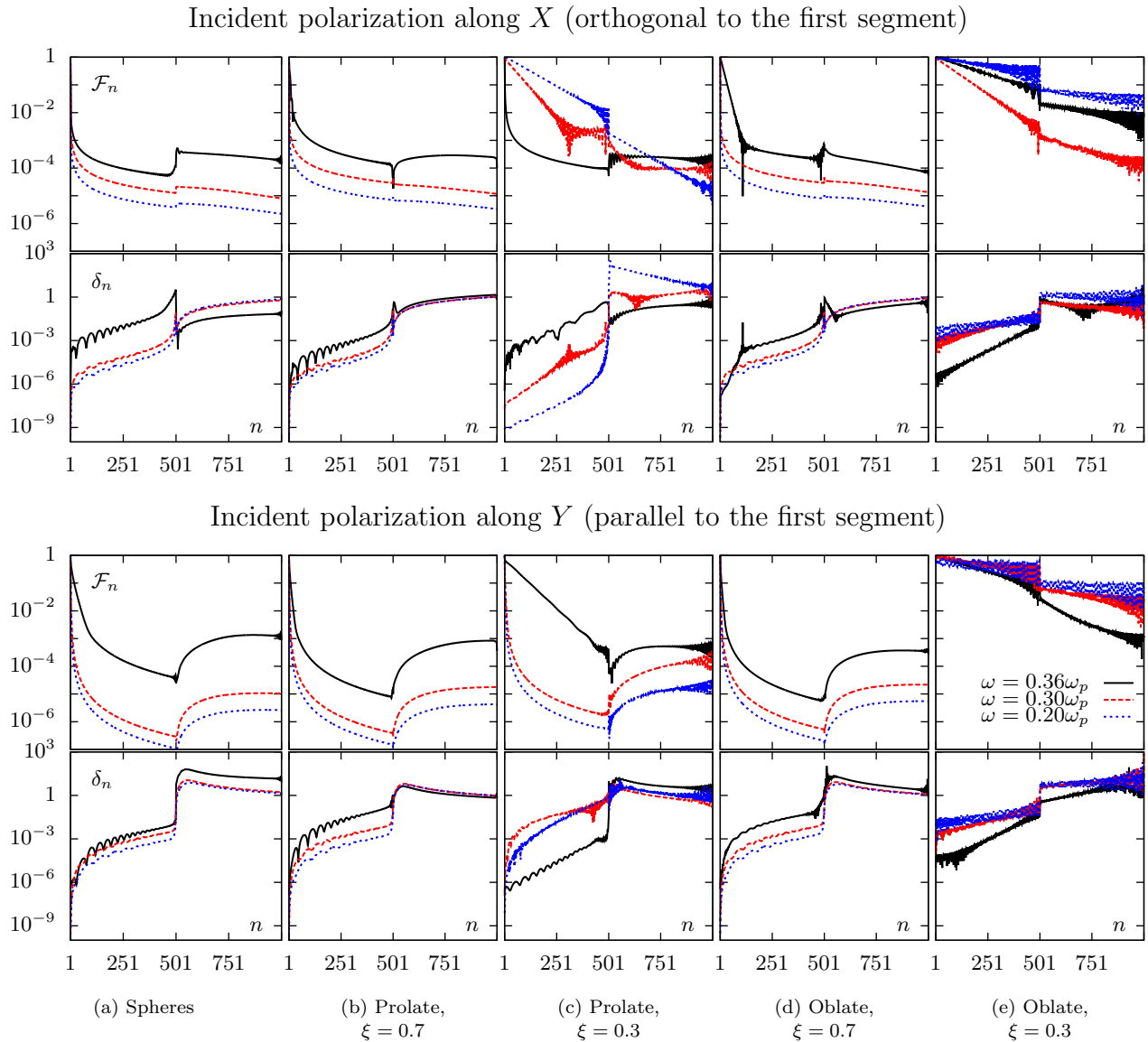
FIG. 2. (Color online) Normalized Green's function $\mathcal{F}_n$ and the depolarization ratio δ_n as functions of the spheroid number in the chain, n, for corner-shaped chains constructed of various types of spheres and spheroids, different working frequencies ω, and different polarizations of the electric field that is incident on the first particle in the chain, as labeled.

with respect to ω. Here the term in the right-hand side is due to second-order dynamic correction to polarizability. Interaction of spheroids in the chain can shift the resonant frequency albeit insignificantly.

A pronounced example of resonant excitation and corresponding exponential decay can be found in chains made of prolate spheroids with $\xi = 0.3$ (Fig. 2). In this case, resonant excitation occurs at $\omega = 0.20\omega_p$ for transverse incident polarization and for $\omega = 0.36\omega_p$ for longitudinal incident polarization. In both cases, the dependence of $\mathcal{F}_n$ on n contains a well-pronounced linear segment in the double-logarithmic scale of the plot. However, for permuted parameters, that is, for $\omega = 0.36\omega_p$ and transverse incident polarization or $\omega = 0.20\omega_p$ and longitudinal incident polarization, the excitation is off-resonance. In this case, the function $\mathcal{F}_n$ drops by several orders of magnitude over just a few chain periods and then undergoes a relatively slow algebraic decay. This behavior

of $\mathcal{F}_n$ has been previously described in linear chains [9,10]. A cross-over from "ordinary" to "extraordinary" SPP, a phenomenon that was also described in these references, can also be observed in Fig. 2 for prolate spheroids with $\xi = 0.3$, $\omega = 0.30\omega_p$ and transverse incident polarization. Finally, we note that the peculiar case of very slow decay, similar to those predicted in Ref. [13], can be observed in the case of oblate spheroids with $\xi = 0.3$.

The above behavior of SPPs is not surprising and has been described previously in linear chains [9,10,13]. What is new and interesting here are the phenomena occurring at the vertex, where the amplitude of the SPP can either decrease or increase sharply. For example, a sharp, almost steplike increase of the amplitude is observed for spheres at the working frequency $\omega = 0.36\omega_p$ (in both incident polarizations). These abrupt changes of the amplitude are, essentially, complex interference effects. The result of practical importance is that

the SPP amplitude at the end of a corner-shaped chain can be significantly larger than in a linear chain of the same overall length.

Another interesting phenomenon that is not observed in linear chains is polarization conversion. It has long been known that diffraction gratings with broken symmetry can facilitate conversion of polarization and that efficiency of this conversion can be greatly enhanced by optical resonances [33]. Almost total conversion of linear polarization by a planar periodic array of L-shaped gold micrometer-sized particles was demonstrated for near-IR light in reflection [34]. The above effects were described for broad-front plane waves. In the case of curved plasmonic chains, we demonstrate polarization conversion for the electromagnetic field of SPP, which is localized in a subwavelength vicinity of a chain. Moreover, the conversion characteristics are fairly flexible. Depending on parameters, a linear polarization can be converted to a nearly perfect circular polarization, or in some cases to a more general elliptical polarization. Reliable linear-to-linear conversion

does not occur in corner chains for the parameters we have considered (but can occur in smooth corners, see below). In the case of oblate spheroids with $\xi = 0.3$, polarization state experiences rapid fluctuations on the scale of about one chain period. We finally note that the effect is reciprocal: an incident circular polarization can be converted by the same chain to a nearly linear polarization.

In the case of a smooth corner (Fig. 3), the effects are similar except that the abrupt changes of the amplitude (which in this case occur at the site where the straight segment is connected to a circular segment) are not as dramatic as in the case of sharp corners. In the case of semicircles (Fig. 4), the SPP amplitude is, generally, a more smooth function of position and does not exhibit abrupt jumps. An interesting observation is that in the case of resonant excitation, a cross-over from ordinary to extraordinary SPP occurs in quarter-circles just like in linear chains, e.g., in prolate spheroids with $\xi = 0.3$, $\omega = 0.36\omega_p$ and incident polarization along Y axis. Finally, semi-circle chains allow in some cases for reliable linear-to-
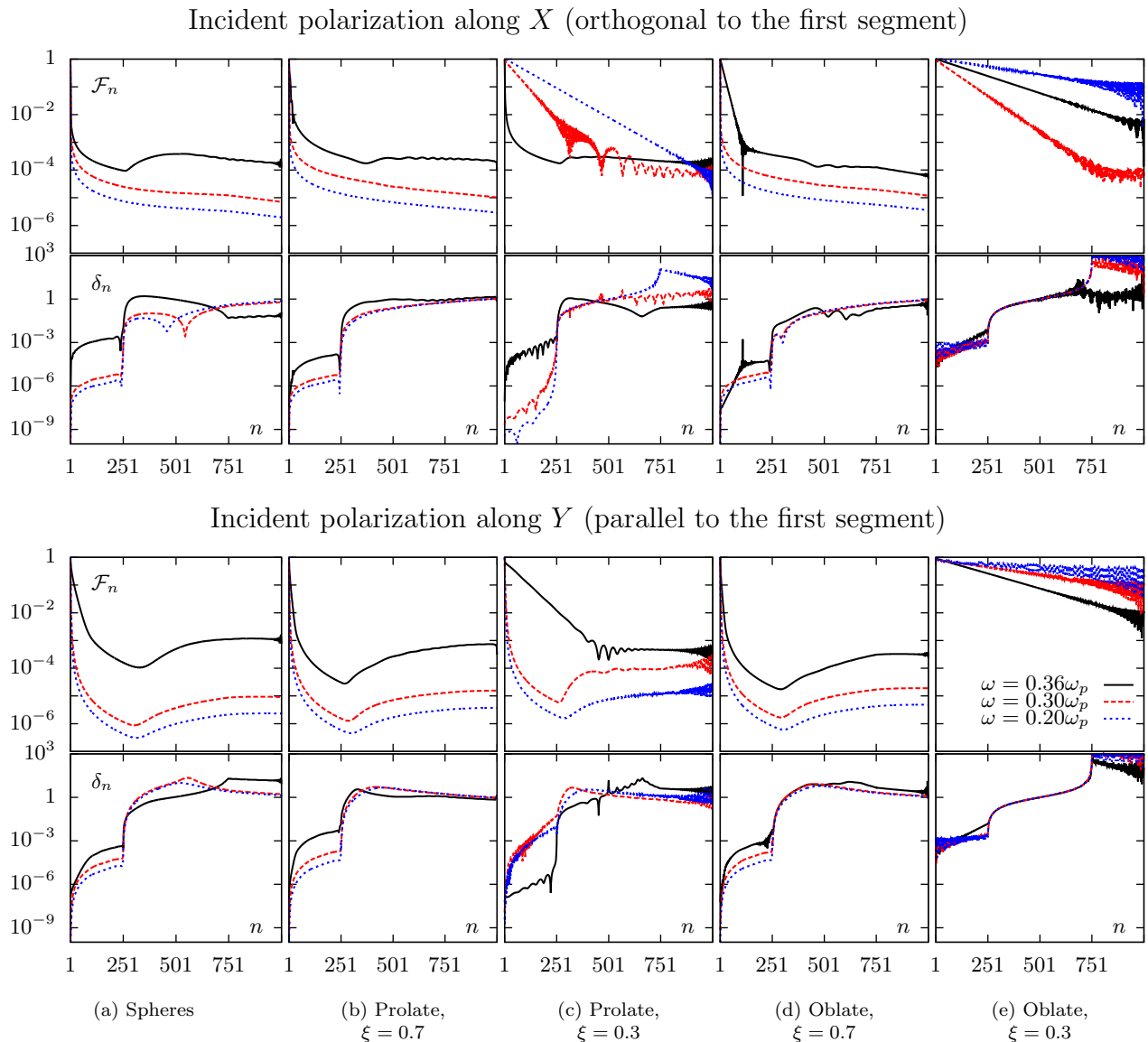

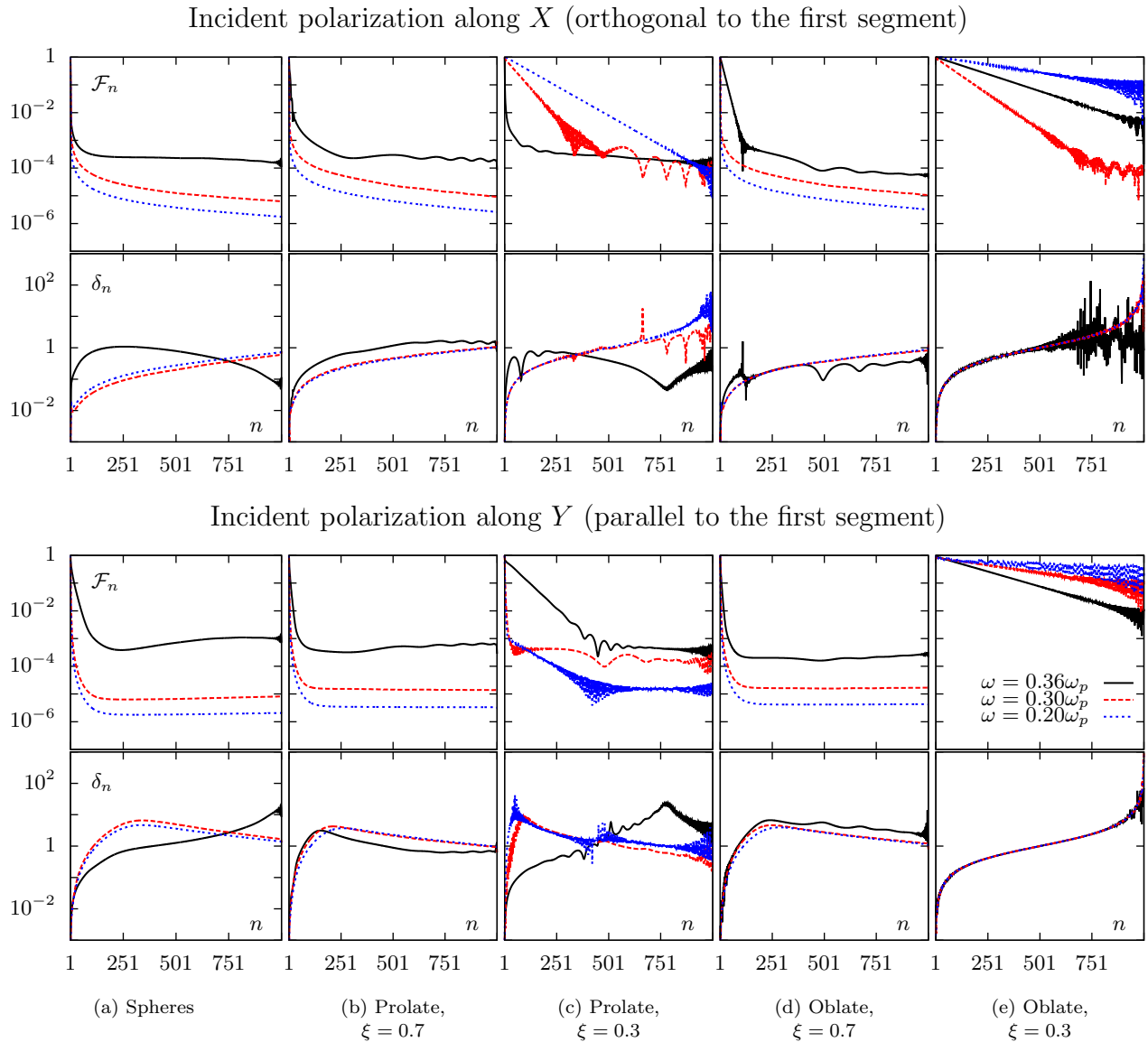FIG. 3. (Color online) Same as in Fig. 2 but for a smooth corner.

Incident polarization along X (orthogonal to the first segment)

Incident polarization along Y (parallel to the first segment)

$$\omega = 0.36\omega_p \quad \text{———}$$
$$\omega = 0.30\omega_p \quad \text{– – –}$$
$$\omega = 0.20\omega_p \quad \text{· · · ·}$$

(a) Spheres

(b) Prolate,
$\xi = 0.7$

(c) Prolate,
$\xi = 0.3$

(d) Oblate,
$\xi = 0.7$

(e) Oblate,
$\xi = 0.3$

FIG. 4. (Color online) Same as in Fig. 2 but for a quarter-circle.

linear polarization conversion. For example, in the case of spheres and $\omega = 0.36\omega_p$, the incident linear polarization along Y axis is smoothly converted to circular polarization close to the middle of the chain and then to linear polarization along X axis at the far end of the chain.

IV. ELECTRIC FIELD LOCALIZATION

We next consider field localization effects. The goal is to show that there are cases when the electromagnetic field associated with an SPP is tightly localized near curved chains (for straight chains, this result is expected). To this end, we have computed the intensity I defined by

$$I = |\mathbf{E}|^2/|\mathbf{E}_1|^2 \qquad (15)$$

at the horizontal plane 10 nm above the top-most points of the spheroids. Note that this plane is located at different heights H above the $z = 0$ plane, depending on the spheroid shape.

Specifically, we have $H = 18$ nm for spheres and prolate spheroids and $H = 37$ nm for oblate spheroids.

We start with the corner chains. In Fig. 5, we show several density plots of $I(x,y)$ for the most interesting cases, which correspond to the chains built from spheroids with relatively small values of aspect ratio and for the working frequency that corresponds to relatively slow decay of SPPs. Note that panel (d) corresponds to the working frequency $\omega = 0.10\omega_p$–a case that is not illustrated in Figs. 2–4 above. It can be seen that better field localization and stable transmission is obtained in the case of oblate spheroids. Scattering and energy leakage at the vortex is insignificant in all cases considered. However, the amplitude decay is very significant in the case of prolate spheroids, so that it is not clear whether a signal can be reliably detected near the end of such chains. (We note that decay in chains made of prolate spheroids is not as significant in the case of quarter-circle chains as is shown below.)

Localization of the electromagnetic field near smooth corner chains is qualitatively similar (Fig. 6). There is visibly
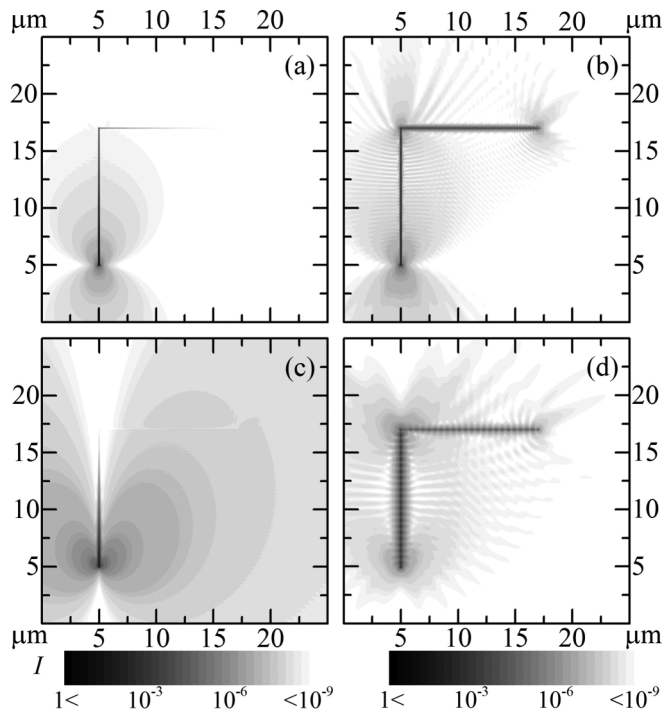
FIG. 5. Density plot of the normalized intensity $I(x,y)$ for corner shaped chains made from prolate (left) and oblate (right) spheroids with the aspect ratio $\xi = 0.3$. The working frequency used is $\omega = 0.20\omega_p$ (a) and (b), $\omega = 0.36\omega_p$ (c), and $\omega = 0.10\omega_p$ (d). Incident polarization along X axis (top) and along Y axis (bottom).

less scattering in this case, localization is somewhat stronger and decay somewhat slower. However, the strongest field localization is obtained in quarter-circle chains (Fig. 7), especially in the case of oblate spheroids. Herein the localization and
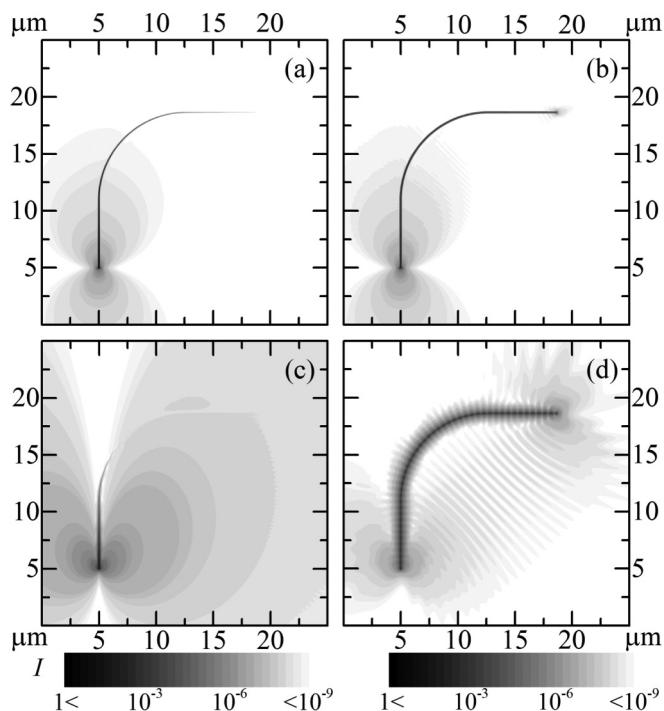

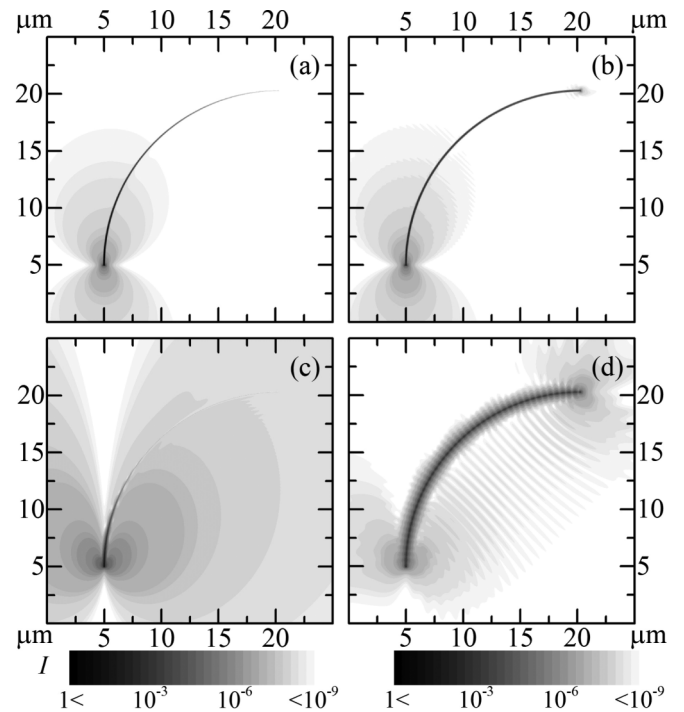FIG. 6. Same as in Fig. 5 but for smooth corner chains.

FIG. 7. Same as in Fig. 5 but for quarter-circle chains.

transmission properties are as good as in the case of straight chains, e.g., as reported in Ref. [13].

V. CONCLUSIONS

We have found numerically that propagation of SPPs in curved chains can be as stable and characterized by similarly strong field localization as in the case of straight chains, as long as the chain shape is smooth. In this case, there is almost no energy leakage due to scattering, just as in the case of a straight chain. This result can be explained by noting that a smooth curved chain can be considered as locally linear, as long as the curvature radius is large enough.

We have further found that SPPs experience much slower decay in chains of spheroids than in similarly shaped chains of nanospheres. The transmission efficiency of nanospheroid chains is two orders of magnitude higher than it is for the case of spheres. The most effective propagation of SPPs (and the strongest field localization) is obtained in chains of oblate spheroids with the aspect ratio $\xi = b/a = 0.3$. In this case, SPPs decay quite insignificantly in very long curved chains, e.g., we obtained for the normalized scalar Green's function $\mathcal{F}_N \gtrsim 0.8$ for sufficiently low excitation frequency.

We finally note that curved chains can be used for efficient and tunable polarization conversion. Linear-to-linear as well as linear-to circular and circular-to-linear conversion is possible.

The physical effects considered in this paper can be observed in near-field experiments with monochromatic or quasi-monochromatic excitation, where polarization sensitivity can be achieved by various types of filters or the use of asymmetric resonant nanoparticles as the near-field probes. The field intensity maps can be observed with the use of leakage radiation microscopy [20,21].

---

[1] A. G. Nikitin, A. V. Kabashin, and H. Dallaporta, Opt. Express **20**, 27941 (2012).

[2] T. V. Teperik and A. Degiron, Phys. Rev. B **86**, 245425 (2012).

[3] T. Cheng, C. Rangan, and J. E. Sipe, J. Opt. Soc. Am. B **30**, 743 (2013).

[4] P. J. Compaijen, V. A. Malyshev, and J. Knoester, Phys. Rev. B **87**, 205437 (2013).

[5] A. G. Nikitin, T. Nguyen, and H. Dallaporta, Appl. Phys. Lett. **102**, 221116 (2013).

[6] C. Lee, M. Tame, C. Noh, J. Lim, S. A. Maier, J. Lee, and D. J. Angelakis, New J. Phys. **15**, 083017 (2013).

[7] R. S. Savelev, A. P. Slobozhanyuk, A. E. Miroshnichenko, Y. S. Kivshar, and P. A. Belov, Phys. Rev. B **89**, 035435 (2014).

[8] A. Vitrey, L. Aigouy, P. Prieto, J. M. Garca-Martn, and M. U. Gonzalez, Nano Lett. **14**, 2079 (2014).

[9] V. A. Markel and A. K. Sarychev, Phys. Rev. B **75**, 085426 (2007).

[10] Y. Hadad and B. Z. Steinberg, Phys. Rev. B **84**, 125402 (2011).

[11] V. A. Markel and A. K. Sarychev, Phys. Rev. B **86**, 037401 (2012).

[12] Y. Hadad and B. Z. Steinberg, Phys. Rev. B **86**, 037402 (2012).

[13] I. L. Rasskazov, S. G. Karpov, and V. A. Markel, Opt. Lett. **38**, 4743 (2013).

[14] B. Auguie and W. L. Barnes, Opt. Lett. **34**, 401 (2009).

[15] D. Van Orden, Y. Fainman, and V. Lomakin, Opt. Lett. **34**, 422 (2009).

[16] K. B. Crozier, E. Togan, E. Simsek, and T. Yang, Opt. Express **15**, 17482 (2007).

[17] A. A. Govyadinov and V. A. Markel, Phys. Rev. B **78**, 035403 (2008).

[18] M. Conforti and M. Guasoni, J. Opt. Soc. Am. B **27**, 1576 (2010).

[19] I. B. Udagedara, I. D. Rukhlenko, and M. Premaratne, Opt. Express **19**, 19973 (2011).

[20] I. P. Radko, S. I. Bozhevolnyi, A. B. Evlyukhin, and A. Boltasseva, Opt. Express **15**, 6576 (2007).

[21] A. B. Evlyukhin, S. I. Bozhevolnyi, A. L. Stepanov, R. Kiyan, C. Reinhardt, S. Passinger, and B. N. Chichkov, Opt. Express **15**, 16667 (2007).

[22] A. B. Evlyukhin and S. I. Bozhevolnyi, Laser Phys. Lett. **3**, 396 (2006).

[23] B. Rolly, N. Bonod, and B. Stout, J. Opt. Soc. Am. B **29**, 1012 (2012).

[24] A. Alu and N. Engheta, Phys. Rev. B **79**, 235412 (2009).

[25] A. B. Evlyukhin, C. Reinhardt, U. Zywietz, and B. N. Chichkov, Phys. Rev. B **85**, 245411 (2012).

[26] M. J. Zheng, D. Y. Lei, K. Yakubo, and K. W. Yu, Plasmonics **6**, 19 (2010).

[27] N. Kinsey, M. Ferrera, G. V. Naik, V. E. Babicheva, V. M. Shalaev, and A. Boltasseva, Opt. Express **22**, 12238 (2014).

[28] Y. N. Gartstein and V. M. Agranovich, Phys. Rev. B **76**, 115329 (2007).

[29] B. Auguie, X. M. Bendana, W. L. Barnes, and F. J. Garcia de Abajo, Phys. Rev. B **82**, 155447 (2010).

[30] A. Moroz, J. Opt. Soc. Am. B **26**, 517 (2009).

[31] V. A. Markel, J. Mod. Opt. **40**, 2281 (1993).

[32] B. T. Draine, Astrophys. J. **333**, 848 (1988).

[33] S. J. Elston, G. P. Bryan-Brown, and J. R. Sambles, Phys. Rev. B **44**, 6393 (1991).

[34] Q. Levesque, M. Makhsiyan, P. Bouchon, F. Pardo, J. Jaeck, N. Bardou, C. Dupuis, R. Hadar, and J. L. Pelouard, Appl. Phys. Lett. **104**, 111105 (2014).